Approaching the Marangoni Effect through equilibrium molecular dynamics

H. G. A. Burton
Robinson College
Cambridge

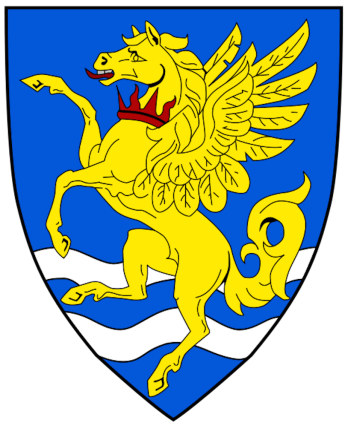

Declaration

This dissertation is submitted in partial fulfilment of the requirements for Part III Chemistry. It describes work carried out in the Department of Chemistry in the Michaelmas Term 2015 and the Lent Term 2016. Unless otherwise indicated, the research described is my own and not the product of collaboration.

Acknowledgements

Acknowledgements will go here.

Approaching the Marangoni Effect through equilibrium molecular dynamics

H. G. A. Burton

Abstract

The Marangoni flow induced by a temperature gradient at a liquid–liquid interface is studied through the use of equilibrium molecular–dynamics simulations for a symmetric Lennard–Jones binary–mixture. An artifical Marangoni force is computed by considering the finite difference in the stress–tensor for two equilibrium simulations at different temperatures. Applying this as a body force to a non–equilibrium simulation at an intermediate temperature allows the Marangoni flow profile to be computed. This is demonstrated for a binary–mixture confined within a piston and a binary–mixture periodic in all dimensions, and the use of the Virial or Irving–Kirkwood stress–tensor is compared. Finally, the method is used to observe the retardation of Marangoni flows due to the addition of surfactant molecules.

Contents

1 Introduction

2015 saw the 160$^{\text{th}}$ anniversary of J. Thompson's report on interfacial flows as the result of a chemical potential or temperature gradient.[1] This phenomenom was later termed the "Marangoni Effet" after it formed the basis of Carlo Marangoni's doctoral dissertation.[2] Since then, temperature induced Marangoni flows, also known as thermocapillary flows, have been the subject of a number of studies and a macroscopic description has been developed through the works of Derjaguin[3] and Levich[4], as summarised in the context of phoresis by Anderson[5].

On the simplest level, this effect can be described as a consequence of a interfacial–tension gradient, with motion occuring from regions of low to regions of high surface–tenson. However, this is not particulaly informative since the temperature dependence of surface–tension is itself known only through empirical studies. Beyond this description, Derjaguin demonstrated that the flow can be calculated from the excess enthalpy of a fluid close to the interface, hence formulating a thermodynamic theory of thermocapillary motion.[3]

The thermodynamic backbone upon which this theory is founded is reliant on knowledge of the macroscopic properties of the system. In contrast, the flow itself is inherently a microscopic phenomenon and is localised at the interfaces of bulk fluids. Such a localised effect cannot be faithfully described using a thermodynamic description, instead it requires a microscopic theory formulated around the interpaticle interactions. No such theory currently exists, and there has been limited research in this area.[6] By studying the microscopic properties of a liqud–liquid interface, this report aims to model the Maragnoni effect and investigate the link between the microscopic fluid properties and its macroscopic motion.

1.1 Experimental studies

Despite the lack of a microscopic theory, there has been substantial experimental research into the Marangoni effect. Many of these studies have focussed on the more curious examples of Marangoni flows, such as Thompson's "tears of wine"[1,7–9] and the "coffee ring effect",[10–12] whilst others have shown it is becoming ever more important in technological applications. For example, Sternling and Scriven[13] proposed Marangoni effects as the origin for interfacial turbelence and mass transport, yielding applications in fluid mixing and oil recovery,[14–16] whilst Subramanian and Balasubramanian outline the importance of Marangoni forces for the motion of bub-

bles and droplets in reduced gravity environments.[17]

In 1959, Young et al. produced a theoretical description of this motion of bubbles and droplets under the influence of a temperature gradient, a phenomena described as thermophoresis.[18] They describe how this gradient causes a higher surface–tension on the low temperature side of the droplet, resulting in a force pulling the surrounding fluid towards the low temperature region and a corresponding reaction force propelling the droplet towards the warmer fluid region (note the similarity to electrophoresis where there is no-net force within the droplet). This force was measured experimentally by S. C. Hardy,[19] who used a temperature gradient to balance the Marangoni and buoyancy forces acting on a droplet within a fluid, thus holding the droplet stationary. Later, theoretical modelling by Kim and Subramanian suggested that the inclusion of surface–active substances could be used to prevent thermophoresis,[20,21] a prediction that was confirmed experimentally.[22,23]

With the advances in space technology over the past half a century, thermophoresis and thermocapillary motion have become important mechanisms for fluid motion and mass transfer in low–gravity environments, where surface effects dominate over buoyancy driven motion. The motion of bubbles and drops due to interfacial gradients is considered to be key for materials processing in space, enabling phase separation of binary mixtures and the potential to make uniform composite materials.[22] Moreover, fluid transport in the absence of gravity is important for controlling fluid fuels aboard satellites, often carried for thrusters used to perform orbital adjustments.[17]

1.2 Striving for a microscopic description

With so many potential applications, the search for a micrcoscpic description is becoming ever more significant, and computer simulations are increasingly being used to understand this phenomenom. Marangoni flows are inherently dynamic and must be studied using a time–dependent method such as molecular dynamics. To model the dynamic behaviour of an immiscible binary–mixture under the effect of a temperature gradient might initially appear trivial; simply create a temperature gradient for such a system and measure the subsequent particle velocites. This non-equilibirum approach is used by Hampe et al. in their study of the Marangoni effect.[6] Despite their positive results, the method is complicated by the use of periodic boundary conditions (required to model a macroscopic fluid) that require each unit cell to have two temperature gradients, such that the temperature is also periodic.

Any flow due to this gradient then generates an opposing concentration gradient and an equilibrium stationary state will be reached.

In this study we investigate the use of equilibirium molecular dynamics simulations for modelling the Marangoni effect. By calculating the equilibrium stress acting on a binary mixture for two different temperatures, the differential of the stress with respect to temperature can be estimated and used to infer a body force corresponding to the Marangoni force. This can then be applied as a constant body force in a non-equilibrium simulation at an intermediate temperature to imitate the Marangoni force, thus circumventing the complications of a periodic temperature profile. Finally, by measuring the velocity profile in this non–equilibrium simulation, the Marangoni flow can be observed.

Using this equilibrium method we show that a Marangoni force at liquid–liquid interface can be calculated from the fluid stress–tensor and used to generate a Marangoni flow. This technique is then used to investigate the effect of surfactants on the magnitude of the Marangoni flow and compare these results to the experimental observations.

The theoretical description of the Maragoni effect is described in Section 2, whilst Section 3 outlines the computational methods used. The simulation results are discussed in Section 4. Section 5 provides a summary of the conclusions and proposes directions for future studies.

2 Theoretical Background

2.1 The macroscopic description

The motion of fluids may be described macroscopically using the Navier–Stokes equation,[24] modelling a liquid as a continuous medium and combining the conservation of mass and momentum with the relation between the force on a volume element and the local fluid flow. In the low Reynolds-number regime the flow velocity is small and thus for a system at equilibrium, the Navier–Stokes equation reduces to

$$\eta \nabla^2 \nu(r,t) = \nabla P(r,t) - \mathbf{f}(r). \tag{1}$$

Crucially, Equation 1 shows that motion in fluids *can only* occur under the presence of a pressure gradient or external forces. In the case of Marangoni flows, motion due to the temperature gradient must results from induced local pressure gradients, which may be derived from thermodynamics.

Consider a binary mixture with an interface at $z = 0$. The Gibbs–Duhem equation gives

$$V \mathrm{d}P = \sum_{i=0}^{n} N_i \mathrm{d}\mu_i + S \mathrm{d}T. \tag{2}$$

In the bulk, the fluid pressure is constant and isotropic, giving

$$\left(\frac{\partial P}{\partial x}\right) = \sum_{i=0}^{n} \rho_i^{\mathrm{B}} \left(\frac{\partial \mu_i}{\partial x}\right) + \frac{S}{V}\left(\frac{\partial T}{\partial x}\right). \tag{3}$$

The Maxwell equations allow the entropy to be related to the partial differential of chemical potential with respect to temperature through

$$\left(\frac{\partial \mu_i}{\partial T}\right)_{P,N_i} = -\left(\frac{\partial S}{\partial N_i}\right)_{P,T}. \tag{4}$$

Now the total entropy is the weighted sum of the partial entropy of the species in the system,

$$S = \sum_{i=0}^{n} s_i N_i, \tag{5}$$

thus

$$\left(\frac{\partial \mu_i}{\partial T}\right)_{P,N_i} = -s_i. \tag{6}$$

Overall, this allows Equation 3 to be expressed as

$$\left(-\sum_{i=1}^{n}\rho_i^{\mathrm{B}}s_i^{\mathrm{B}}+\frac{S^{\mathrm{B}}}{V}\right)\left(\frac{\partial T}{\partial x}\right) \tag{7}$$

for which the solution is trivially

$$\frac{S^{\mathrm{B}}}{V}=\sum_{i=1}^{n}\rho_i^{\mathrm{B}}s_i^{\mathrm{B}}. \tag{8}$$

Consider the case close to an interface or surface where the pressure will deviate from its bulk value. Assuming μ_i and T are such that

$$\left(\frac{\partial \mu_i}{\partial T}\right)=-s_i^{\mathrm{B}} \tag{9}$$

remains true, the pressure gradient reduces to

$$\left(\frac{\partial P(z,x)}{\partial x}\right)=\left(\sum_{i=1}^{n}\rho_i(z)\left(s_i(z)-s_i^{\mathrm{B}}\right)\right)\left(\frac{\partial T}{\partial x}\right). \tag{10}$$

In the case of an ideal mixture, the partial entropy is given by $s_i=\frac{\mu_i-h_i}{T}$, and since μ_i and T are independent of z, the pressure gradient can be expressed in terms of the excess enthalpy, $\Delta h(z)$,

$$\left(\frac{\partial P(z,x)}{\partial x}\right)=-\Delta h(z)\frac{1}{T}\left(\frac{\partial T}{\partial x}\right)=-\Delta h(z)\left(\frac{\partial \ln T}{\partial x}\right). \tag{11}$$

Substituting Equation 11 into Equation 1 and assuming there is no pressure gradient in either the z or y direction allows the velocity at the interface to be computed as

$$\nu(z=0)=-\frac{1}{\eta}\int_0^{\infty}\mathrm{d}z\, z\Delta h(z)\frac{\partial T}{\partial x} \tag{12}$$

where it has been assumed that the fluid in the bulk is at rest ($\nu_x(z=\infty)$) is at rest. This expression is almost equivalent to that derived by Derjaguin et. al., except for a factor of two, suggesting there may be an error in Derjaguin's approach.[3,5]

2.2 A microscopic approach

By its very nature the Marangoni effect is a phenomenom which occurs on microscopic lengthscales, and hence this macroscopic hydrodynamical approach is not

entirely appropriate. Instead of solving the Navier–Stokes equation, the velocity field should be related directly to the local forces acting on the fluid, which may be calculated from the local stress tensor,

$$f_x(z) = -\left(\frac{\partial \sigma_{xx}(z,x)}{\partial x}\right). \tag{13}$$

In the case of Marangoni flows, the force is due to a temperature gradient and $f_x(z)$ can be calculated from the chain rule as

$$f_x(z) = -\left(\frac{\partial \sigma_{xx}(z,x)}{\partial T}\right)\left(\frac{\partial T}{\partial x}\right). \tag{14}$$

2.3 The Finite Difference Approach

Equation 14 shows that the body force due to a temperature gradient can be inferred from the temperature variation of the stress–tensor. To first order, the temperature gradient of the stress–tensor can be calculated using a finite difference approach as

$$\left(\frac{\partial \sigma_{xx}(z,x)}{\partial T}\right) \approx \frac{\sigma_{xx}^{T_2}(z,x) - \sigma_{xx}^{T_1}(z,x)}{T_2 - T_1}. \tag{15}$$

Using this approximation, the Marangoni flow profile can be computed as follows:

1. Compute $\sigma_{xx}(z)$ for an equilibrium system at a given temperature T_1.
2. Repeat the calculation for another equilibrium system at slightly higher temperate T_2.
3. Approximate the temperature gradient of the stress tensor using the finite difference approach (Equation 15).
4. Infer $f_x(z)$ using Equation 14 to calculate a force profile.
5. Compute the flow profile by applying $f_x(z)$ as an artifical body force to a non-equilibrium simulation at an intermediate temperature T_3 (i.e. $T_1 < T_3 < T_3$).

2.4 Non-uniqueness of the pressure tensor

The stress tensor is intimately related to the pressure tensor as

$$\sigma_{\alpha\beta}(\mathbf{r}) = -P_{\alpha\beta}(\mathbf{r}). \tag{16}$$

The pressure tensor can be considered as a sum of two contribtuions, a kinetic part arising from the momentum transfer of the particles on the container walls and potential part attributed to the intermolecular forces.[25] The kinetic part may be calculated from the ideal-gas contribution,

$$\mathbf{P}^K(\mathbf{r}) = k_\mathrm{B}T\rho(\mathbf{r})\hat{\mathbf{I}}, \tag{17}$$

whilst the potential contribution cannot be uniquely defined.

For a homogeneous fluid system, the stress tensor is isotropic, with each diagonal element equal to $-P$, where P is the bulk hydrostatic pressure. This pressure can be calculated using the Virial equation, originally derived from the Virial theorem of Clausius[26], (although also derivable by differentiating the canonical partition function[27]) to give

$$P_{\alpha\beta}(\mathbf{r}) = \frac{1}{V}\left(\rho(\mathbf{r})\left\langle\nu_\alpha\nu_\beta\right\rangle + \frac{1}{2}\sum_{i\neq j}(r_\alpha^{(i)} - r_\alpha^{(i)})f_\beta^{ij}i\right). \tag{18}$$

Clausius' formulation calculates the local pressure by considering the forces acting on particles located within a volume element at $\mathbf{r}$.

In an inhomogeneous system, such as one containing a liquid–liquid interface, there is an ambiguity over which particles should contribute to the force at a given position.[25,27,28] This was first reported by Irving and Kirkwood[29,30] who describe an alternative method that computes the pressure tensor from the forces acting across an infinitesimal surface d$\mathbf{A}$ located at $\mathbf{r}$. They calculate the local pressure tensor using only pairs of particles for which the line connecting their centers of mass passes through d$\mathbf{A}$. For planar systems, such a those involving an interface in the (x, y) plane, the pressure tensor depends only on the distance from this interface and the normal and tangential components of the pressure tensor can be expressed as

$$P_\mathrm{N}^\mathrm{IK}(z) = \rho(z)k_\mathrm{B}T - \frac{1}{2A}\left\langle\sum_{i\neq j}\frac{|z_{ij}|}{r_{ij}}U'(r_{ij})\Theta\left(\frac{z-z_i}{z_{ij}}\right)\Theta\left(\frac{z_j-z}{z_{ij}}\right)\right\rangle, \tag{19}$$

$$P_\mathrm{T}^\mathrm{IK}(z) = \rho(z)k_\mathrm{B}T - \frac{1}{4A}\left\langle\sum_{i\neq j}\frac{x_{ij}^2+y_{ij}^2}{r_{ij}}\frac{U'(r_{ij})}{|z_{ij}|}\Theta\left(\frac{z-z_i}{z_{ij}}\right)\Theta\left(\frac{z_j-z}{z_{ij}}\right)\right\rangle. \tag{20}$$

The Irving–Kirkwood has distinct advantages over the Virial method for studying planar systems, in particular it yields a normal component independent of local fluctuations in the number density. For planar systems, density fluctuations occur close to walls due to structural layering of the fluid, and there is reduced density at

liquid–liquid interfaces from the finite width of the interfacial region. As a result, oscillations in the normal component of the Virial pressure are observed in such systems[25] whilst the Irving–Kirkwood pressure yields a constant normal component, equal to the bulk hydrostatic pressure. This is more consistent with the expected result since the fluid is isotropic in the direction normal to the surface.

3 Computational Methods

Equilibrium molecular dynamics simulations of a symmetric binary–mixture of two immiscible fluids (A and B) were used to measure the stresses acting on the fluid at two different temperatures and infer the Marangoni force using Equation 15. Where possible, this force was then applied as an artificial body force to generate a Marangoni flow profile at an intermediate temperature.

Two key systems were studied, a symmetrical binary–mixture under three–dimensional periodic boundary conditions, and a binary–mixture periodic in two–dimensions but confined between two walls in the third-dimension, as shown in Figure 1. All molecular dynamics simulations were executed using the LAMMPS (Large Atomic and Molecular Massively Parallel Simulator) package.[31]

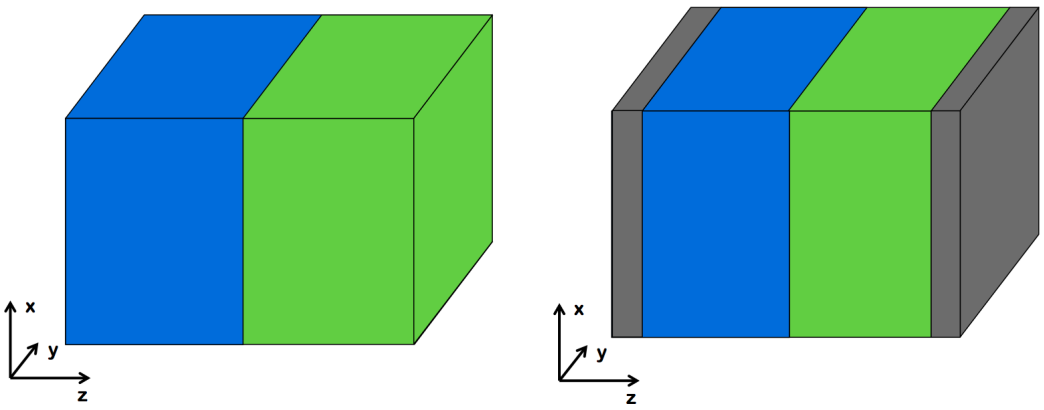

Figure 1: The system arrangements for a symmetric binary–mixture of two immiscible fluids under three-dimensional periodic boundary conditions (left) and a binary–mixture periodic in two–dimensions held within two walls (right) are shown. In the case of the three–dimensional boundary conditions, pressure must be controlled use a Nosé–Hoover barostat whilst for the fluid confined between two walls, these walls may be used as a piston to control the fluid pressure.

3.1 Interaction Model

The fluids were modelled using spherical particles and their interaction was controlled through a pair–wise truncated Lennard–Jones potential:

$$V\left(\mathbf{r}^{\mathrm{N}}\right) = \frac{1}{2}\sum_{i\neq j}\phi\left(r_{ij}\right) \tag{21}$$

where

$$\phi\left(r_{ij}\right) = 4\epsilon_{ij}\left(\left(\frac{\sigma_{ij}}{r_{ij}}\right)^{12} - \left(\frac{\sigma_{ij}}{r_{ij}}\right)^{6}\right) \text{ for } r < r_c \tag{22}$$

$$\phi\left(r_{ij}\right) = 0 \text{ otherwise.} \tag{23}$$

This potential involves an attractive r_{ij}^{-6} term accounting for the long–range Van der Waal's interaction and a short–range r_{ij}^{-12} repulsion term corresponding to the Pauli repulsion between particles. The length–scale of the potential is given by σ_{ij} (chosen to be equal for all pairs of i and j) whilst the parameter ϵ_{ij} determines the strength of the interaction.

The miscibility of the two fluids (A and B) can be controlled using the relative values of the interaction parameter, in this study the values chosen were:

$$\epsilon_{A,A} = \epsilon_{B,B} = 1.0, \tag{24}$$

$$\epsilon_{A,B} = 0.55, \tag{25}$$

in agrement with previous studies on immiscible symmetrical Lennard–Jones binary mixtures.[6,32,33] The cutoff for the Lennard–Jones potential was chosen to be $r_c = 4\,\sigma$.

Physical quantities including distances and energies are expressed in terms of reduced units. For a Lennard–Jones system, the basic units are σ for length, ϵ for energy and m for mass, from which all other units may be derived.[34] Physical quantities become dimensionless when expressed in terms of these units, for example $r^* \equiv r/\sigma$. Scaled coordinates expressed relative to the simulation box size are also used, for example $z' = z^*/L_{z^*}$ where L_{z^*} is the dimension of the box in the z–direction. These are useful if the box–dimensions vary, such as when a barostat acts on the system.

3.2 Thermostats

In molecular dynamics simulations, the temperature is controlled using thermostats, which simulate the coupling of the system to an external heat bath.

Thermostats work by applying a stochastic frictional force to particles, either by adding a random force to momenta (Langevin)[35] or reassinging the velocity of randomly chosen particles from the Maxwell distribtuion (Anderson)[36]. The Nosé–Hoover thermostat was used throughout this study. This adds an extra term into the equations of motion to provide the effect of an external heat bath.[37–39] The result

is a system where the energy fluctuates but the combined energy of the system and heat bath remains constant, maintaining a canonical ensemble.

3.3 Barostats

The bulk pressure of the fluid must also be held constant. A piston provides the simplest method and is relatively easy to create; the fluid is confined between two solid walls and a force equal to P_{ext}/A_{wall} is applied. This was used for studing the binary–mixture confined between two planar walls. In the case of Marangoni flows, a thermocapillary effect will also occur at the boundary of the liquid and the solid piston. If the thermocapillary force can be ignored, and non–slip wall boundary conditions exist, then a piston also allows the bulk fluid to be fixed at rest.

Alternatively a Nosé–Hoover barostat can control the pressure by adjusting the box dimensions and altering the equations of motion.[37–39] When studying surface effects, the box dimensions must only be changed in the direction perpendicular to the interface, since any other direction will alter its area and create an error in the thermodynamic pressure,

$$P = -\left(\frac{\partial F}{\partial V}\right)_T + \gamma\left(\frac{\partial A}{\partial V}\right)_T. \tag{26}$$

3.4 Preparing the system

The fluid was prepared from a face–centred cubic lattice with a spacing of 1.64414 σ and a simulation box size of $L_{x^*} = 13.1531$, $L_{y^*} = 13.1531$ and $L_{z^*} = 32.8828$. This lattice was equilibrated over 2×10^6 timesteps of length 0.001 τ to generate a fluid state. The barostat was set to a pressure of $P^* = 0.1$ and the temperatures used were $T^* = 0.8$ and $T^* = 0.9$, ensuring the system occupied the liquid region of the Lennard–Jones phase space.[40] Solid walls in the system were represented by a harmonically bonded lattice with spring constant of $K^* = 2500$ and an equilbrium length of $r_0^* = 1.163$.

3.5 Calculating the stress–tensor

The Virial stress–tensor was calculated using an in–built function within the LAMMPS package, which returns the stress–tensor for each atom. However, LAMMPS does not have a method for calculating the Irving–Kirkwood stress–tensor. Instead this was calculated by dumping the particle positions on a given timestep to a file and

post–processing. The stress–tensor was then computed using a programme written by R. Ganti and adapted for the specific systems studied. This was significantly more expensive than the Virial stress–tensor, incurring approximately a 4-fold increase in computational time.

3.6 Computing averages

Usually time–averages of physical observables are calculated in molecular dynamics simulations. In the systems studied, the relevant observables corresponded to the number–density, stress–tensor and particle velocities. Their values were measured every timestep and spatially averaged for 400 planar slabs across the z–dimension of the box. These spatial averages were then time–averaged over the full duration of the simulation.

Under the ergodic hypothesis, time–averages can be equated to ensemble averages for an infinitely long simulation time.[41] Practically, however, these averages must be evaluated over a finite time period and have an associated statistical error. The method of block–averaging, developed by Flybjerg and Peterson, provides an efficient technique for computing this error.[42] They show that the variance of an observable, A, can be estimated by

$$\mathrm{var}(A) \geq \left\langle \frac{C_0}{n-1} \right\rangle , \tag{27}$$

where C_0 is the value of the time-correlation function for the block–transformed data at $t = 0$ and is given by

$$C_0 \equiv \frac{1}{n} \sum_{k=1}^{n} \left(A_k - \bar{A}\right) \left(A_k - \bar{A}\right) . \tag{28}$$

A lower bound for the variance can be calculated by finding the block length at which this estimate reaches a plateau. Furthermore, the error in the variance can be estimated as

$$\sqrt{\frac{2}{n-1} \times \frac{C_0}{n-1}}. \tag{29}$$

A blocking–analysis for a binary–mixture identical to those used throughout this study was executed over a simulation time of $1,000\ \tau$ and $10,000\ \tau$, as shown in Figure 2. The plateau begins at a block length of $10\ \tau$ for the long simulation and $5\ \tau$ for the shorter run, with little increase in the error of the variance until a much larger block size. Considering this result, a block length of $10\ \tau$ was used to provide a good estimate for the error of all time–averages calculated in the subsequent simulations.

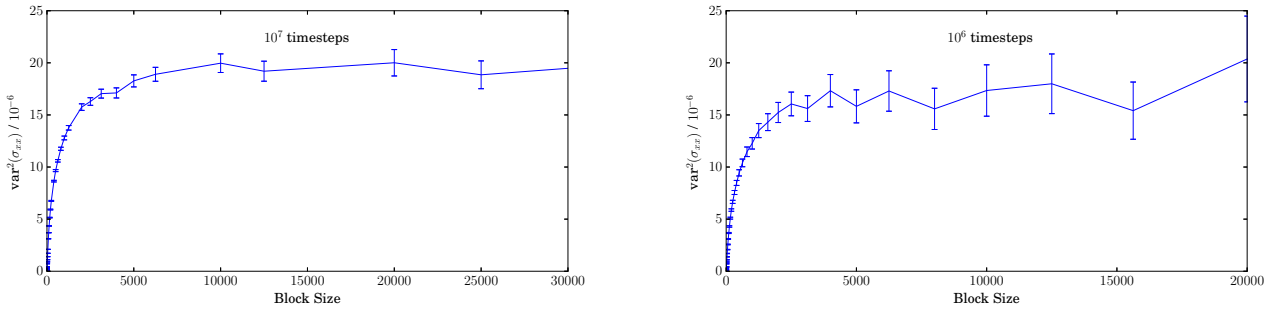

Figure 2: The blocking analysis for a simulation time of 10,000,000 timesteps and 1,000,000 timesteps shows clear plateaus in the estimate of the error at block sizes of 10,000 and 5,000 respectively. This can be used to estimate the size of blocking needed to decorrelate data in the corresponding molecular dynamics simulations.

3.7 Modelling surfactant molecules

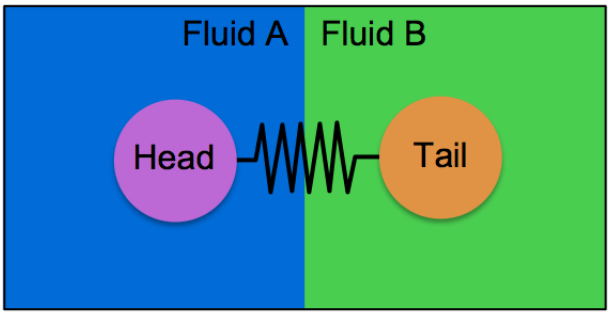

Figure 3: Surfactant molecules are represented by a pair of Lennar–Jones spherical particles connected by a harmonic bond. The head particle has a stronger interaction with fluid A whilst the tail has a stronger interaction with fluid B. These properties are controlled using the relative values of ϵ_{ij} and imitate the typical behaviour of non–ionic surfactant molecules.

To investigate the effects of surfactants on the Marangoni effect, the surfactant molecules were modelled as a pair of Lennard–Jones particles connected by a harmonic bond with spring constant $K^* = 25$ and equilibrium bond length $r_0^* = 1.63$. Inspired by Howes and Radke's study on non–ionic surfactants,[43] the 'head' particle has a stronger interaction with fluid A particles, ($\epsilon_{H,A} = 1.33$ and $\epsilon_{H,B} = 0.17$) whilst the 'tail' particle has a stronger interaction with fluid B particles ($\epsilon_{T,A} = 0.17$ and $\epsilon_{T,B} = 1.33$). The 'head' and 'tail' groups interact with each other with strength

$\epsilon_{H,T} = 1.00$.

3.8 Software details

All molecular dynamics simulations were carried out using the LAMMPS (Large Atomic and Molecular Massively Parallel Simulator) package.[31] Additional processing was carried out using Numpy.[44] All graphical figures were plotted using Matplotlib.[45]

4 Results and Discussion

4.1 Binary–mixture confined between two walls

Initially, a binary–mixture of two fluids confined between two walls was studied. The fluid was prepared as described in Section 3.4 at a pressure of $P^* = 0.1$ and temperatures of $T^* = 0.8$ and $T^* = 0.9$. The confining walls were used as a piston to control the pressure.

4.1.1 Using the Virial stress

Once equilibrated, the simulations were run for 40×10^6 timesteps and the number–density and Virial stress–tensor were computed every timestep. These values were then time-averaged to produce profiles for the number–density and $\sigma_{xx}(z')$ as shown in Figures 4 and 5.

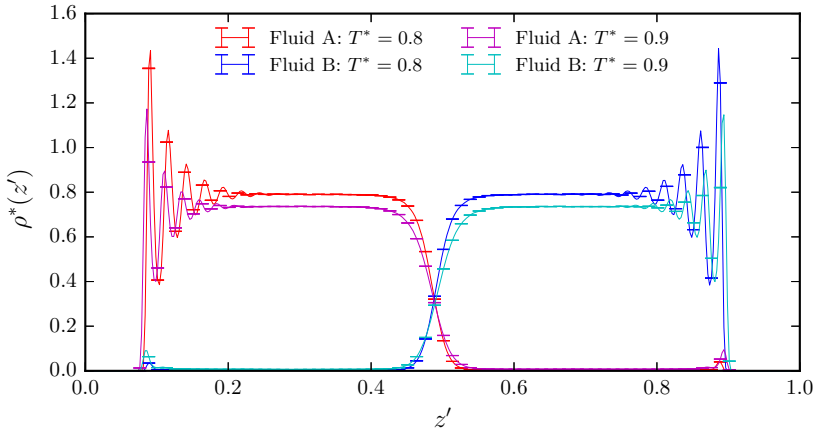

Figure 4: The number density for the two fluids at $T^* = 0.8$ and $T^* = 0.9$ is shown. The bulk density is uniform, representing a fluid state, and the interface can be seen as the sharp change in the densities of the two fluids. Near the wall there are oscillations in the density, representing structural layering of the fluid.

Both the density profile and the stress–profile show the expected features of a binary–mixture. There is a uniform density in the bulk of the fluid and an interfacial region of finite width where the density of one species falls sharply and the density of the other increases. Close to the walls, there are large oscillations in the density that are a consequence of structural layering in the fluid close to the solid.

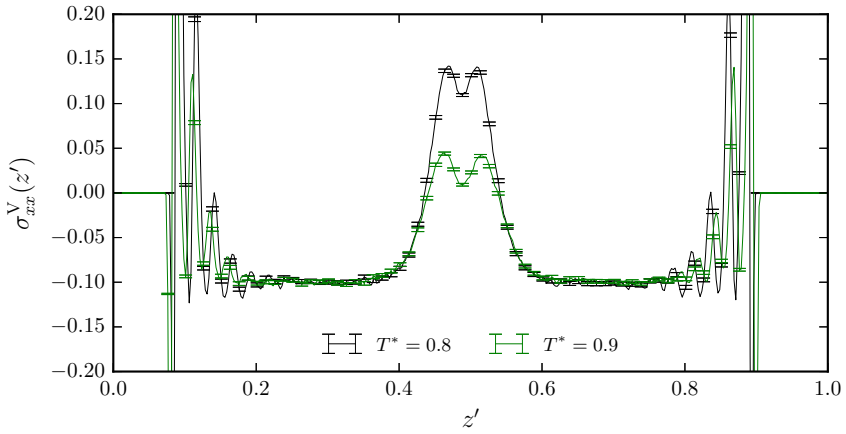

Figure 5: The Virial stress tensor for the total fluid at each temperature shows a bulk value equal to $-P_{ext}$, representing the hydrostatic pressure, and a peak at the interface due to the anisotropy of the interparticle forces in this region. This peak is related to the interfacial tension and its temperature dependence is the driving force for the Marangoni effect. Towards the wall there are temperature dependent oscillations which may provide the origin of the thermocapillary force.

For the stress–profile, the bulk value for the tangential component is equal to $-P_{\text{ext}}$, corresponding to the hydrostatic pressure of the fluid. At the interface there is a peak in the tangential stress due to the anisotropy of the intermolecular forces in this region; this can be related to the interfacial tension.[46]

The time–averaged values for the stress–tensor were then used to estimate the gradient of the stress with respect to temperature using Equation 15, as shown in Figure 6. This gradient also shows a peak at the interface of the two fluids, providing the origin of the Marangoni force. Importantly the gradient in the bulk of the fluid (far from both the interface and the walls) is zero, within statistical error, ensuring there is no force acting in the bulk fluid. In addition, there is an oscillating gradient at the surface of the wall which can be interpreted as a thermocapillary force. Since we are only interested in simulating the Marangoni effect, these thermocapillary forces were ignored.

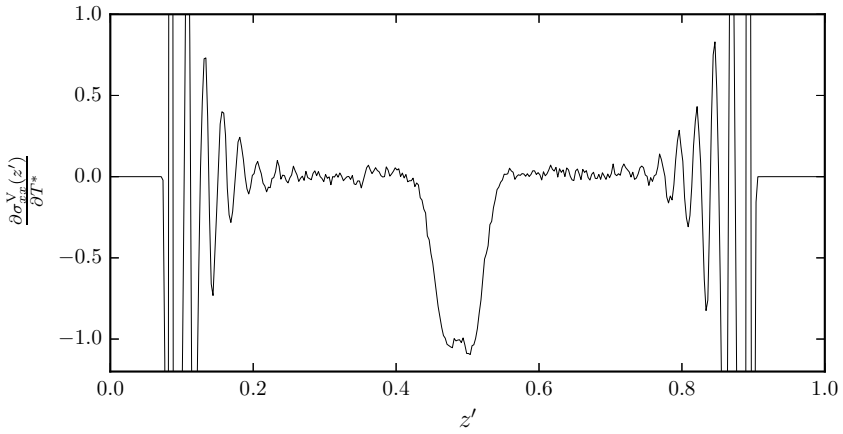

Figure 6: The gradient of the Virial stress–tensor with respect to temperature shows a negative peak at the interface. This will generate a force in the opposite direction to a temperature gradient, creating a Marangoni flow. The oscillations at the liquid–solid boundaries create a thermocapillary force and are ignored.

The central 1/3 of the force profile was then used to create an artifical Marangoni force using a temperature gradient of $\partial T^*/\partial x^* = 0.001$ and Equation 14. This artfical body force was applied to an identical system prepared at $T^* = 0.85$. A non-equilibrium simulation was then run for 40×10^6 timestpes and the time–average of the x–component of the fluid velocity, $v_x^*(z')$, was computed. The momenta of the walls in the x and y directions were fixed such that they provided a stationary reference point for the fluid. As a result, the fluid shows non-slip boundary conditions and the walls act to hold the bulk fluid at rest.

The flow profile calculated for the fluid in this system is shown in Figure 7. There is a sharp negative peak at the interface indicating a Marangoni flow in the opposing direction to the temperature gradient. Furthermore, the flow decays linearly away from the interface, consistent with a Couette flow arising from shear–driven fluid motion.[47] There is also a net flow of the fluid, suggesting an overall force acting on the liquid. The walls in the system act as a momentum sink, providing a friction force on the fluid which allows this steady–state flow to arise under the isolated effect of a temperature–gradient.

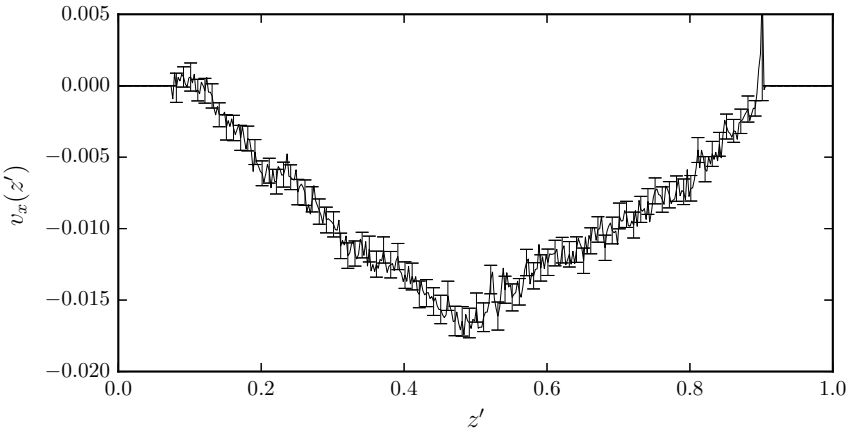

Figure 7: The fluid velocity generated from a non–equilibrium simulation with an applied artifical Marangoni force calculated from the Virial stress shows a peak at the interface. The flow direction of this peak is from warm regions to cold. The greatest velocity magnitude is around 0.16 and this decays linearly to zero at the surface of the piston, corresponding to a Couette flow.

4.1.2 Comparing to the Irving–Kirkwood stress

Figure 4 shows there are significant deviations in the fluid density at the interface and the walls and that the amount of deviation varies with temperature. Because of the strong dependence of the Virial stress on the local density of the fluid, there is the potential for these changes to interfere with the measurement of the Marangoni force. To verify the significance of these deviations, the stress–tensor was also calculated using the Irving–Kirkwood formula, since this does not depend on the local fluid density.

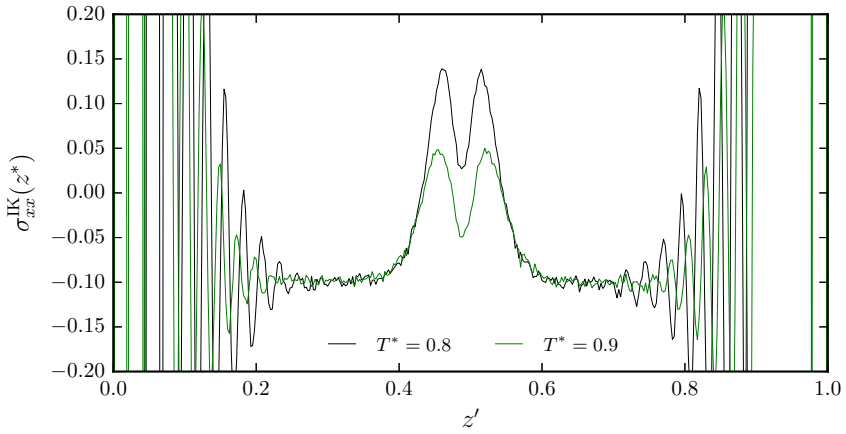

Figure 8: The Irving–Kirkwood stress–tensor shows a similar profile to the Virial stress–tensor (see Figure 5) although the interfacial peak is divided into two and a reduction in the stress occurs directly at the interface. There are also similar oscillations at the wall due to a thermocapillary force.

The fluids were prepared at $P^* = 0.1$ and $T^* = 0.8$ and $T^* = 0.9$ as before. Since the Irving–Kirkwood stress–tensor takes much longer to compute (see Section 3.5), the equilibrium simulations were only run for 1×10^6 timesteps, resulting in a greater amount of statistical error. This produced the time–averaged stress–tensor profiles shown in Figure 8.

The finite difference method was again used to calculate the gradient of this stress–tensor with respect to temperature and this is compared to the Virial result in Figure 9. Still focussing on only the central 1/3 of the fluid, there is a good correspondence between the two gradient profiles and the interfacial peak occurs both across the same spatial region and with the same maximum value. The most signifcant difference occurs directly at the interface, where there is a sharp reduction in the Irving–Kirkwood gradient. This is probably a result of the reduction in density at the interface affecting the Virial stress–tensor more than the Irving–Kirkwood stress–tensor.

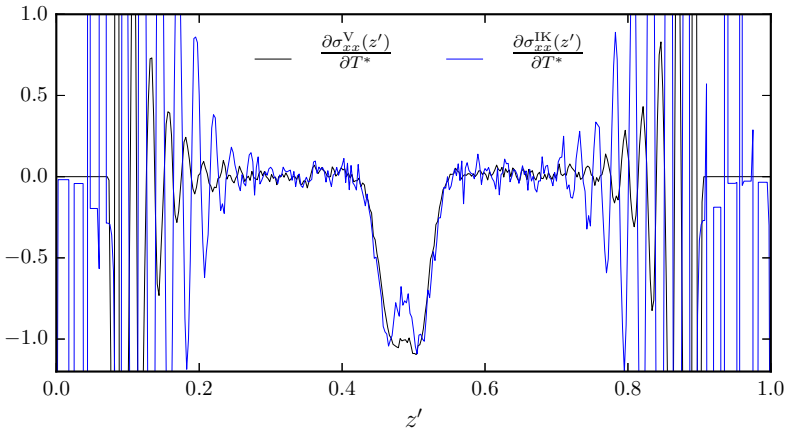

Figure 9: The gradient of the Irving–Kirkwood stress–tensor with respect to temperature shows a peak across the interfacial region, representing the origin of the Marangoni force. This occurs with a similar maginitude to the gradient of the Virial stress–tensor although like the stress profile, the Irving–Kirkwood gradient is split into two peaks. In both gradient profiles, there is no net gradient in the bulk and thus there will be no body force acting in the fluid bulk.

Using a temperature gradient of $\partial T^*/\partial x^* = 0.001$ to compute the Irving–Kirkwood aritifical body force, a non–equilibrium simulation at $T^* = 0.85$ was run for 40×10^6 timesteps. The flow profile was calculated and compared to the result obtained using the Virial force, as shown in Figure 10. The profiles show a reasonably good correspondence, especially for the region $z' \leq 0.4$, although they deviate for higher values of z'. In particular the flow from the Irving–Kirkwood force is not as large directly at the interface, as a result of the reduction in the force at this point. The Irving–Kirkwood velocity profile is also asymmetric despite the symmetry of the system. This asymmetry may be the result of an increase in the noise of the Irving–Kirkwood force relative to the Virial force, which results from the shorter simulation time enforced by the high computational cost of the Irving–Kirkwood analysis.

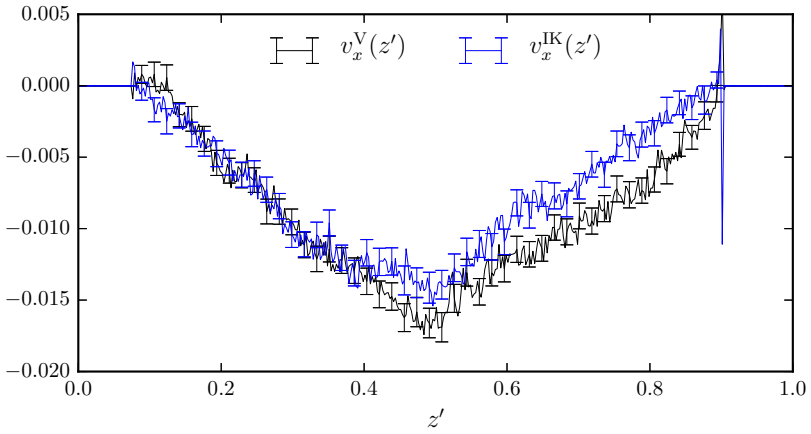

Figure 10: The flow profile calculated using the Irvining–Kirkwood Marangoni flow shows a similar profile to that calculated from the Virial force, with a sharp peak at the interface and a linear Couette flow into the bulk. The peak value is not as large as that from the Virial force as a result of the sharp reduction of the Irving–Kirkwood stress gradient directly at the interface. The Virial flow is symmetric whilst the Irving–Kirkwood flow is not, this is probably a result of the greater degree of noise in the Irving–Kirkwood gradient due to a short simulation time.

4.2 Binary–mixture periodic in 3-dimensions

Equation 1 showed that the existence of a temperature gradient in the system should not be able to generate a net flow in the fluid. Levich discusses this further, describing how the interfacial flow must be accompanied by a back-flow in the bulk fluid.[4] In the case of the binary–mixture held between two walls, the stationary walls provide a momentum sink which allows a net flow to exist within the fluid. To replicate the behaviour described by Levich, a system void of momentum sinks must be studied, for example a binary–mixture of two immiscible fluids with periodic boundary conditions in all dimensions.

This system, shown on the left–hand side of Figure 1, was prepared as described in Section 3.4 with the parameters given in Section 3.1. The distance between consecutive interfaces was $0.5L_{z^*}$. A Nosé–Hoover barostat and thermostat were used to control the pressure at $P^* = 0.1$ with temperatures of $T^* = 0.8$ and $T^* = 0.9$.

4.2.1 Comparing the Virial and Irving–Kirkwood stress

There is again an ambiguity over which stress–tensor should be used for computing the Marangoni force. Initially, the equilibrated symmetric binary–mixture was simulated for 10×10^6 timesteps and the number–density, σ^{V} and σ^{IK} were computed. As discussed before, the Irving–Kirkwood analysis was highly computationally expensive and this simulation length was the upper feasible limit.

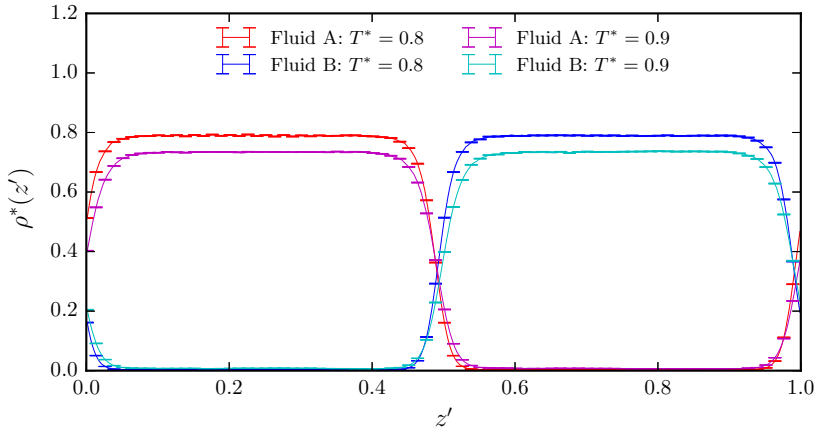

Figure 11: The number–density of the component fluids at $T^* = 0.8$ and $T^* = 0.9$ shows a binary–mixture with the interface at around $z' = 0.5$. With the periodic boundary conditions, there are two interfaces per simulation box. The number density falls at higher temperature and the position of the interface is slightly shifted, this shift must be removed before calculating the stress–gradient.

After this period, the density profile (plotted in Figure 11) showed a uniform density in the fluid bulk and a sharp interfacial region as expected. However, the exact position of the interface had shifted during the simulation and was no longer coincedent for the two temperatures. To calculate the Marangoni force from the stress profile, this shift was manually removed by recentering the interfaces prior to computing the finite difference.

The recentered Virial and Irving–Kirkwood stress profiles are plotted in Figures 12 and 13 respectively. As with the fluid confined between two walls, the bulk stress–tensor components are equal to $-P_{\mathrm{ext}}$, correpsonding to the hydrostatic fluid pressure. There is a similar peak in both the Virial and Irving–Kirkwood stress at the interface. The peaks also have the same maximum value for both stress–tensors, although the Irving–Kirkwood stress shows a stronger minimum directly at

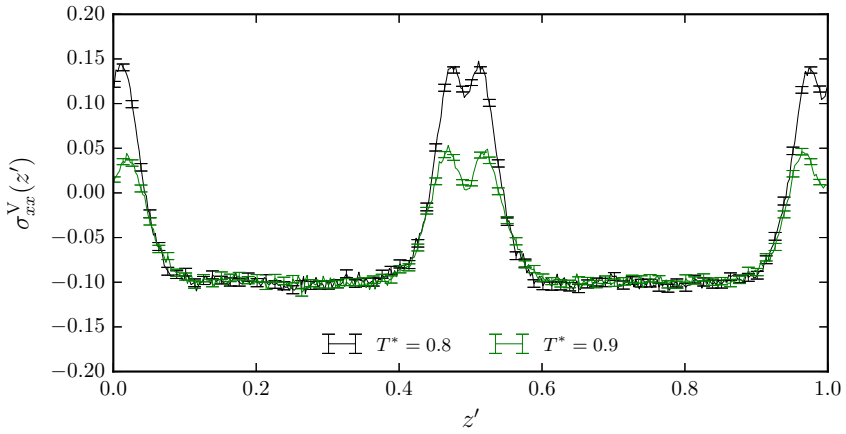

Figure 12: The tangential component of the Virial stress–tensor shows a bulk value of $-P_{ext}$ and a peak at the interfaces due to the anisotropy of the interparticle fluids at these points. This peak has a similar form to that seen in the fluid confined between two wall, seen in Figure 5.

the interface. Similarly to Figure 8, this is probably the result of a reduced density in the interfacial region.

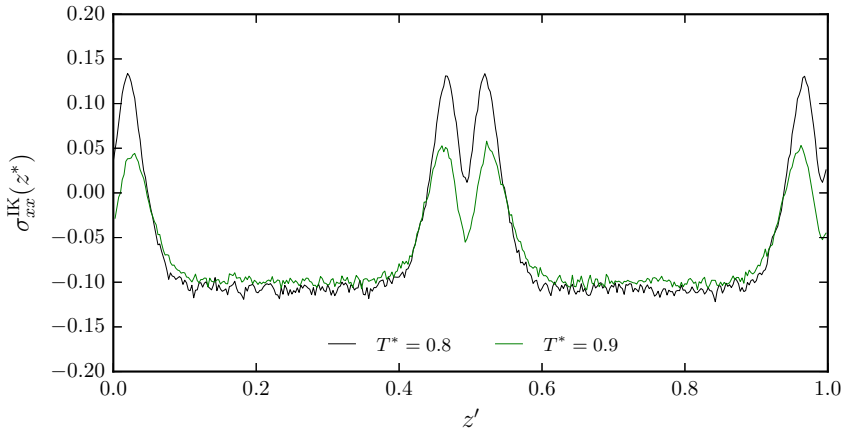

Figure 13: Similarly to Figure 8, the Irving–Kirkwood stress for the binary–mixture periodic in three dimensions matches the Virial stress closely except directly at the interfaces. The Irving–Kirkwood and Virial stress both show peaks of a similar magnitude and spatial coverage but the peak in the Irving–Kirkwood stress is again split into two peaks.

Using these stress profiles, the gradient of the stress with respect to temperature was calculated through the finite difference approach. For there to be no net force acting on the fluid, the gradient profile was adjusted by subtracting the average value from each point to ensure the intergral over all space was zero, as shown in Figure 14. This replicated the effect of a momentum sink in the infinite periodic fluid, for example a distant bounding wall.

The resulting gradient profile shows a similar peak at the interface to Figure 9. The maximum values are similar, suggesting that fixing the total force to zero correctly adjusts the data to give a physically meaningful Marangoni force. Again there is a reasonably good correspondence between the gradient calculated from the Irving–Kirkwood and Virial stress–tensors, and the magnitude of the Irving–Kirkwood peak is reduced directly at the interface. There is also a bulk gradient acting in the opposite direction to the interfacial peak, generating the predicted back force which balances the Marangoni force. However, the profile as a whole shows too much noise for the fine–structure to be determined and is not of a sufficient quality to be used in calculating an artificial body–force.

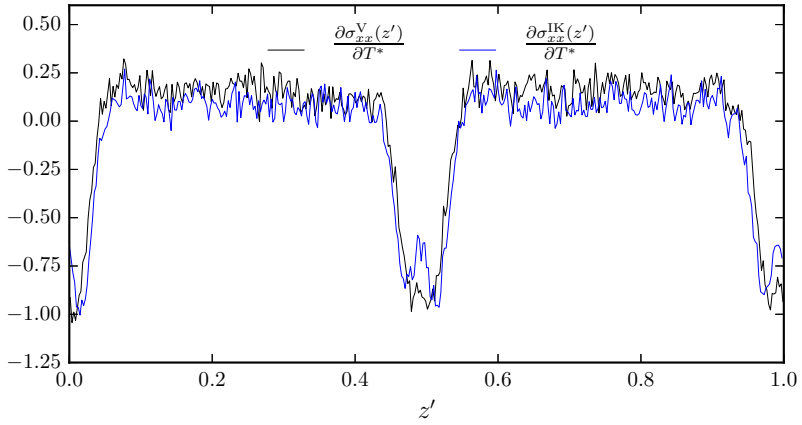

Figure 14: The gradient of the stress–tensor with respect to temperature calculated using equilibrium simulations of 10×10^6 timesteps shows the expected peak at the interfaces. This profile was adjusted to give no net gradient by subtracting the average gradient. There appears to be a good correspondence between the Irving–Kirkwood and Virial stress–gradients, however such a short simulation timescale gives a large amount of noise in this gradient profile. Consequently, the gradient profiles are not sufficiently precise to use for calculating an artificial body force and applying this to a non–equilibrium simulation.

4.2.2 Reducing the noise in the force–profile

To generate a gradient profile with a sufficiently low level of nosie requires either a larger system size or a longer simulation time. Both of these increase the computational cost of calculating the Irving–Kirkwood stress–tensor beyond a practical level, and the Virial stress–tensor must be used. Considering how similar the Virial and Irving–Kirkwood gradient profiles appear in Figure 9, using the Virial stress–tensor does not create too much deviation from the more suitable Irving–Kirkwood stress–tensor, whilst enabling a much longer simulation time.

The reduced noise stress–profile was generated by running the equilibrium systems for 30×10^6 timesteps. Recentering the interfaces generated the Virial stress profile shown in Figure 15. For both temperatures, the profiles show much less noise compared to Figure 12, especially in the bulk region, and the interfacial peaks are more symmetric.

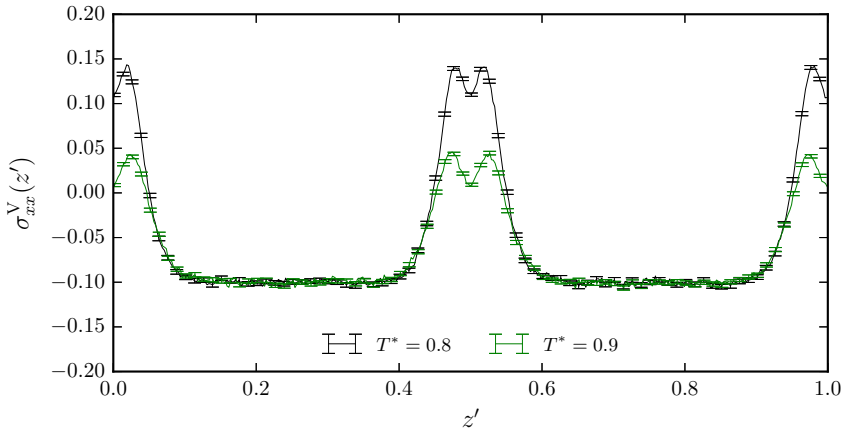

Figure 15: Running the equilibrium simulation over 30×10^6 timesteps produced a much more precise Virial stress profile with a significant reduction in noise relative to Figure 12. The noise in the bulk stress lies within statistical error and thus is consistent with the hydrostatic pressure. This simulation time is too long for the Irving–Kirkwood method to be feasible.

Using these stress profiles, the gradient of the stress–tensor with respect to temperature was again computed using the finite difference and the average value subtracted to give the profile shown in Figure 16. There is a dramatic reduction in the noise of this gradient profile compared to Figure 14, with a sharp peak at the interface and an opposing gradient in the bulk regions.

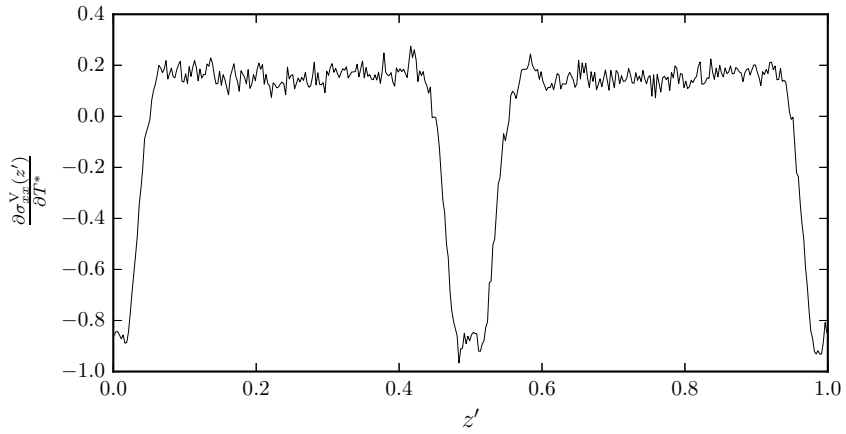

Figure 16: The Virial stress gradient calculated using equilibrium simulations of 30×10^6 timesteps showed significantly less noise than the equilibrium simulations of 10×10^6 timesteps. Having subtracted the average value to give no gradient overall, the plot confirms there is a sharp and symmetrical interfacial peak with an opposing gradient in the fluid bulk.

Using the gradients given in Figure 16 and a temperature gradient of $\partial T^*/\partial x^* = 0.001$, an artifical body force was computed. The body force was recentered to ensure that the peak corresponding to the Marangoni force aligned with the interfacial region, and was applied in a non–equilibrium simulation at $T^* = 0.85$. This simulation was run for 40×10^6 timesteps, and $v_x^*(z')$ was computed to give the flow profile plotted in Figure 17.

Despite the simulation being run for a long timescale, this flow profile still retains a lot of statistical noise. It would be difficult practically to reduce this noise further. Moreover, the average velocity (indicated the hashed line) is non–zero, implying that there is centre–of–mass motion during the simulation. This motion is occuring even though the gradient–profile has been recentered to give no net force overall. It is likely that in the absence of a momentum sink for a system like this, it would be very difficult to completely remove this net flow without artificially fixing the centre–of–mass throughout the simulation.

Despite this, the relative motion across the fluid can still be considered, and there does appear to be a velocity peak at the interface (with $v < v_{\mathrm{COM}}$) corresponding to a Marangoni flow with a back flow in the bulk fluid (with $v > v_{\mathrm{COM}}$) as predicted. This result is, however, somewhat ambiguous and there was insufficient project time to improve the non–equilibrium simulation further.

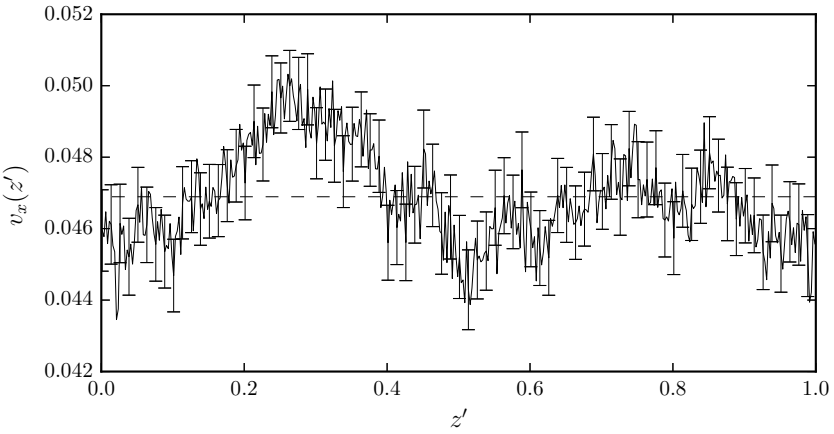

Figure 17: The flow profile calculated from a non–equilibrium simulation using the stress gradient shown in Figure 16 and a temperature gradient of $\partial T^*/\partial x^* = 0.001$ has a large amount of noise and is not very conclusive. There is a net flow velocity despite the average gradient being set to zero, it is unlikely this could be improved upon without artificially fixing the centre–of–mass. Despite this, the fluid velocity relative to this centre–of–mass motion suggests a negative peak at the interfaces with some back flow in the bulk regions, satisfying Levich's requirement of a stationary net flow.[4]

4.3 The effect of surfactants

Surfactant molecules decrease the surface free energy of interfaces, as they have a favourable interaction with both fluids and bridge the interfacial plane. This reduction in surface–tension should also cause a decrease in the Marangoni effect, as observed experimentally.[20–23]

To model this, the non–ionic surfactant molecules described in Section 3.7 were added to the binary–mixture confined between two walls. This system was chosen since the results of Section 4.1 showed it allowed a steady–state flow to be generated and modelled effectively.

The surfactant molecules were added to a single plane between the two fluids in the initial lattice before equilibration. A certain fraction of these molecules were then removed to vary the surfactant concentration, quantified as a fraction of the total number of fluid particles present,

$$\text{Surfactant Fraction} \equiv \frac{N_{\text{surfactant}}}{N_{\text{surfactant}} + N_{\text{fluid}}}. \tag{30}$$

This allowed the surfactant fraction to be varied between 0 and 0.00323.

Taking surfactant fractions of 0.000, 0.0031, 0.0098, 0.0194, 0.0264, 0.0298 and 0.0323, the fluid was then prepared as described in Section 3.4, with a pressure of $P^* = 0.1$ and temperatures of $T^* = 0.8$ and $T^* = 0.9$. A piston barostat and Nosé–Hoover thermostat were used and each system was run at equilibrium for 30×10^6 timesteps of length 0.001 τ.

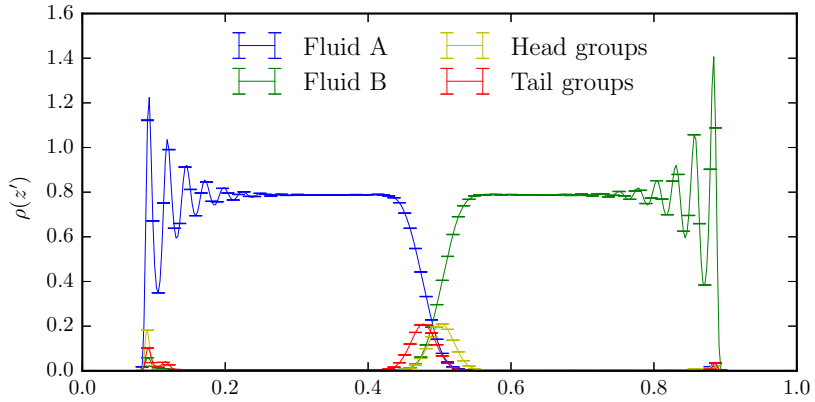

Figure 18: The number density for the binary–mixture with nonionic surfactant molecules, at $T^* = 0.8$ and with a surfactant fraction of 0.0194, is plotted. There is a uniform density in the bulk, showing a fluid like state, and a sharp interface where the densities of Fluid A and Fluid B change rapidly. The surfactant particles are localised at the interface with a low solubility. They also show the correct orientation, with 'Head' particles interacting most strongly with Fluid A and 'Tail' particles with Fluid B.

The resulting number density of each species shows a uniform bulk density, a sharp interface and peaks for the head and tail groups located at the interface, as shown for $T^* = 0.8$ and a surfactant fraction of 0.0194 in Figure 18. The surfactant molecules were correctly oriented with head groups interacting with fluid A and tail groups with fluid B.

The Virial stress–tensor was computed during the equilibrium simulations and used to compute the gradient of the stress with respect to temperature for each surfactant fraction. These results, plotted in Figure 19, show a pronounced reduction in the magnitude of the interfacial peak as the surfactant fraction increases. This corresponds to the expected reduction in the Marangoni force at the interface. Two smaller positive peaks on either side of the centre also develop for higher surfactant

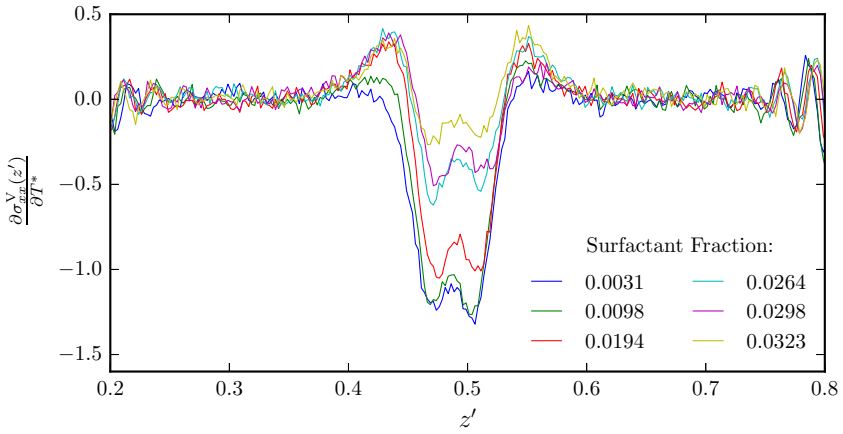

Figure 19: The gradient of the Virial stress–tensor for the surfactant systems still shows a strong interfacial peak for a low surfactant fraction. As the amount of surfactant is increased, the strength of this peak decreases to zero with a resulting reduction in the Marangoni force.

fractions. These potentially correspond to an opposing force driven by a gradient in the amount of surfactant at the interface, which becomes significant at high surfactant fractions. Further investigation would be needed to confirm the origin of this peak.

Using a temperature gradient of $\partial T^*/\partial x^* = 0.001$, the central 1/3 of the stress–gradients in Figure 19 were used to caculate an artificial body force, which was applied in a non–equilibrium simulation at $T^* = 0.85$. These simulations were run for 30×10^6 timesteps over which $v_x(z')$ was computed and plotted in Figure 20. There is a clear decrease in the interfacial velocity as the surfactant fraction is increased, suggesting that the presence of surfactants is causing a retardation of the Marangoni effect.

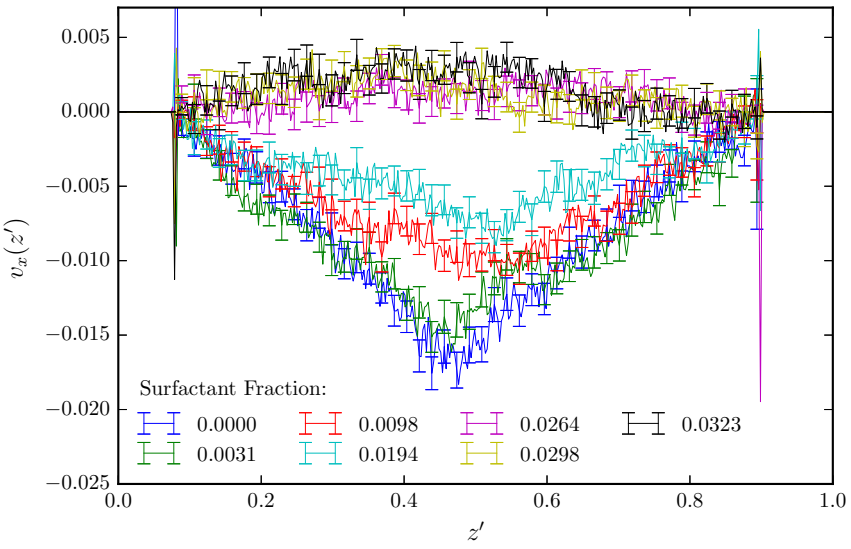

Figure 20: For a low surfactant fraction, the flow profile closely resembles that of the non–surfactant system with an interfacial peak and a linear decay into the bulk. As the amount of surfactant increases there is a reduction in the magnitude of this peak until the Marangoni flow is essentially removed.

The interfacial velocity can be taken as the peak velocity of the profiles shown in Figure 20. Comparing these values against the surfactant fraction shows a clear reduction in the magnitude of this peak value as the surfactant fraction increases, as shown in Figure 21. Above a fraction of 0.025 it appears the Marangoni effect has been removed completely, matching the experimental observations well.

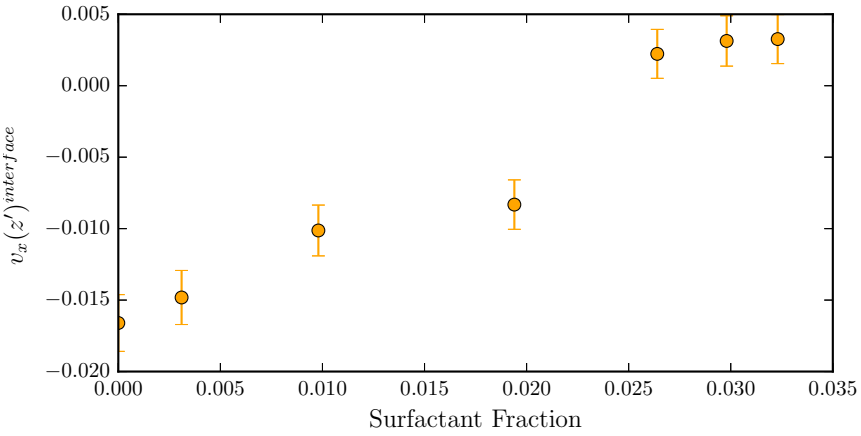

Figure 21: As the surfactant fraction in the system increases, the magnitude of the interfacial velocity decreases. Above a fraction of 0.025, this velocity is essentially zero, although there is small velocity in the opposite direction to the Marangoni flow. This backwards velocity may be the result of a gradient in the amount of surfactant at the interface, which could occur as the surfactant molecules will be more soluble at higher temperatures so will have a smaller interfacial excess. Such an effect may only be significant for high surfactant concentrations.

The sharpness of the peak in the Marangoni flow is also decreased and no longer fits the Couette model as conclusively as when no surfactant molecules are present. This may be because the surfactant molecules decrease the viscosity at the interface, giving non-uniformity across the fluid. To confirm this, the viscosity could be measured using the Green–Kubo relation,

$$\eta = \frac{1}{V k_{\mathrm{B}} T} \int_0^\infty \left\langle \sigma_{xy}\left(\tau\right) \sigma_{xy}(0) \right\rangle \mathrm{d}\tau. \tag{31}$$

This would form a good basis for future work in this area.

5 Concluding Remarks

Using equilibrium simulations at two close temperatures, the gradient of the stress–tensor with respect to temperature was estimated for binary–mixtures through a finite–difference method. This gradient was calculated for the Virial and Irving–Kirkwood stress–tensors for a binary–mixture confined between two walls, and in both cases there was a similar negative peak at the interface. Combining with a temperature gradient, an artificial body force was calculated and applied in a non–equilibrium simulation, yielding a net interfacial flow that was interpreted as the Marangoni effect. The flow occured in the opposing direction to the temperature gradient as predicted. Despite no external forces acting on the system, a net steady state flow was possible since the confining walls provided a momentum sink and a balancing frictional force.

The same method was then applied for a binary–mixture which was periodic in all three–dimensions, and a similar peak in the stress–gradient was measured. However, there was a large amount of noise in this gradient which was reduced by running the simulation for a longer time period. As a result, only the Virial stress was feasible for calcualting a sufficiently precise gradient profile. To create the effect of a momentum sink in this infinite fluid, the stress–gradient was adjusted such that the overall gradient was zero. Applying this force in a non–equilibrium simulation produced a flow profile, showing a negative peak at the interfaces relative to a net centre–of–mass motion, and an associated back flow in the bulk of the fluid. Whilst there should be no overall flow in this system, it is likely that the noise in the applied force created errors which resulted in the net fluid motion.

To remove these effects, one would either need to reduce the noise in the force profile or create a more effective artificial momentum sink. Reducing the noise further would require even longer simulation times which could introduce other errors through the divergence of molecular dynamics simulations. Alternatively, it could be possible to fix the momentum by holding the centre–of–mass stationary throughout the simulation, although this may obscure other important physical features.

Having established a working system in the form of the fluid confined between two walls, the effect of surfactants on Marangoni flows was investigated by adding different concentrations of non-ionic surfactant molecules. The Virial stress was again computed at two temperatures and its gradient was estimated through the finite difference method. As the concentration of surfactant increased, there was a

reduction in the magnitude of the interfacial peak.

These stress–gradients were used to calculate an artificial body force that was then applied in a non–equilibrium simulation. The resulting Marangoni flow was seen to decrease to zero as the surfactant concentration increased, in agreement with experimental studies. Furthermore, the shape of the velocity profile deviated from the linear decay observed in the absence of surfactant. This may be due to a non–uniform fluid viscosity, since the addition of surfactants should also decrease the viscosity of the interfacial region.

In future studies, it would be interesting to compute the viscosity of different regions in the fluid and compare them to the flow velocity. In addition, the change in the Marangoni flow profile due to reduced interfacial viscosity could be studied by using a different pairwise interaction for each fluid. For example, using a potential with no attractive component for one fluid and a Lennard–Jones potential for the other would create an interfacial region with greater anisotropy of the interparticle interactions, causing the viscosity to change. Fine–tuning each potential would also allow greater control over the variation in viscosity.

Through the results of this study combined with future work, a greater understanding of the relationship between the stresses within a fluid and the velocity due to a temperature gradient can be achieved. Ultimately this is working towards a comprehensive microscopic understanding of the Marangoni effect.

References

1. J. Thompson, *Phil. Mag.* **10**, 330 (1855).

2. C. Marangoni, *Ann. der Phys* **22**, 337 (1871).

3. B. V. Derjaguin, N. V. Churaev, and V. M. Muller, *Surface Forces*, Consultants Bureau, 1987.

4. V. G. Levich, *Physiochemical Hydrodynamics*, Prentice–Hall, 1962.

5. J. L. Anderson, *Ann. Rev. Fluid Mech.* **21**, 61 (1989).

6. H. A. Maier, P. A. Bopp, and M. J. Hampe, *Can. J. Chem. Eng.* **90**, 833 (2012).

7. D. C. Venerus and D. N. Simavilla, *Scientific Reports* **5**, 16162 (2015).

8. R. Tadmor, *J. Colloid Interface Sci.* **332**, 451 (2009).

9. R. Vuilleumier, V. Ego, L. Neltner, and A. M. Cazabat, *Langmuir* **11**, 4117 (1995).

10. F. Girard, M. Antoni, and K. Sefiane, *Langmuir* **24**, 9207 (2008).

11. H. Hu and R. G. Larson, *J. Phys. Chem. B* **110**, 7090 (2006).

12. K. Sefiane, *Adv. Colloid Interface Sci.* **206**, 372 (2014).

13. C. V. Sternling and L. E. Scriven, *AIChE J.* **5**, 514 (1959).

14. A. D'Aubeterre, R. da Silva, and M. E. Aguilera, *Int. J. Heat Mass Transf.* **32**, 677 (2005).

15. P. Lyford, H. Pratt, F. Greiser, and D. Shallcross, *Can. J. Chem. Eng.* **76**, 167 (1998a).

16. P. Lyford, H. Pratt, F. Greiser, and D. Shallcross, *Can. J. Chem. Eng.* **76**, 175 (1998b).

17. R. S. Subramanian and R. Balasubramanian, *The motion of bubbles and drops in reduced gravity*, Cambridge University Press, 2001.

18. N. O. Young, J. S. Goldstein, and M. J. Block, *J. Fluid Mech.* **6**, 350 (1959).

19. S. C. Hardy, *J. Colloid Interface Sci.* **69**, 157 (1979).

20. H. H. Kim and R. S. Subramanian, *J. Colloid Interface Sci.* **127**, 417 (1989a).

21. H. H. Kim and R. S. Subramanian, *J. Colloid Interface Sci.* **130**, 112 (1989b).

22. K. D. Barton and R. S. Subramanian, *J. Colloid Interface Sci.* **133**, 211 (1990).

23. J. Chen and K. J. Stebe, *J. Fluid Mech.* **340**, 35 (1997).

24. J.-P. Hansen and I. R. McDonald, *Theory of Simple Liquids*, Academic Press, 4 edition, 2013.

25. F. Varnik, J. Bachnagel, and K. Binder, *J. Chem. Phys.* **113**, 4444 (2000).

26. R. Clausius, *Phil. Mag.* **40**, 122 (1870), Engl. Trans.

27. J. S. Rowlinson and B. Widom, *Molecular Theory of Capillarity*, Clarendon Press, 1982.

28. J. P. R. B. Walton, D. J. Tildesley, J. S. Rowlinson, and J. R. Henderson, *Mol. Phys.* **48**, 1357 (1983).

29. J. G. Kirkwood and F. P. Buff, *J. Chem. Phys.* **17**, 338 (1949).

30. J. H. Irving and J. G. Kirkwood, *J. Chem. Phys.* **18**, 817 (1950).

31. S. Plimpton, *J. Comp. Phys* **117**, 1 (1995).

32. E. Diaz-Herrera, G. Ramirez-Santiago, and J. A. Moreno-Razo, *J. Chem. Phys.* **123**, 184507 (2005).

33. F. J. Martínez-Ruiz, A. I. Moreno-Ventas Bravo, and F. J. Blas, *J. Chem. Phys.* **143**, 104706 (2015).

34. D. Frenkel and B. Smit, *Understanding Molecular Simulation*, Academic Press, 2 edition, 1996.

35. Schneider and Stoll, *Phys. Rev. B* **17**, 1302.

36. H. C. Anderson, *J. Chem. Phys.* **72**, 2384 (1980).

37. S. Nosé, *Mol. Phys.* **52**, 255 (1984).

38. S. Nosé, *J. Chem. Phys.* **81**, 511 (1984).

39. W. Hoover, *Phys. Rev. A* **31**, 1695 (1985).

40. B. Smit, *J. Chem. Phys.* **96**, 8639 (1992).

41. P. A. Bopp, J. B. Buhn, H. A. Maier, and M. J. Hampe, *Chem. Eng. Comm.* **195**, 1437 (2008).

42. H. Flyvbjerg and H. Petersen, *J. Chem. Phys.* **91**, 461 (1989).

43. A. J. Howes and C. J. Radke, *Langmuir* **23**, 1835 (2007).

44. S. van der Walt, S. C. Colbert, and G. Varoquaux, *Comput. Sci. Eng.* **13**, 22 (2011).

45. J. D. Hunter, *Comput. Sci. Eng.* **9**, 90 (2007).

46. A. Marchand, J. H. Weijs, J. H. Snoeijer, and B. Andreotti, *Am. J. Phys.* **79**, 999 (2011).

47. B. S. Massey, *Mechanics of Fluids*, CRC Press, 9 edition, 2012, Revised by J. Ward–Smith.